Fabrication tolerant high-speed SiP ring modulators and optical add-drop multiplexers for WDM applications

Nojić, Jovana, Sharif Azadeh, Saeed, Müller, Juliana, Merget, Florian, Witzens, Jeremy

Jovana Nojić, Saeed Sharif Azadeh, Juliana Müller, Florian Merget, Jeremy Witzens, "Fabrication tolerant high-speed SiP ring modulators and optical add-drop multiplexers for WDM applications," Proc. SPIE 11285, Silicon Photonics XV, 112850A (26 February 2020); doi: 10.1117/12.2543324

SPIE.

Event: SPIE OPTO, 2020, San Francisco, California, United States

Fabrication tolerant high-speed SiP ring modulators and optical add-drop multiplexers for WDM applications

Jovana Nojić[*a], Saeed Sharif Azadeh[a,b], Juliana Müller[a], Florian Merget[a], Jeremy Witzens[a]

[a]Institute of Integrated Photonics, RWTH Aachen University, Campus Blvd. 73, Aachen, Germany;
[b]Now at Max Planck Institute of Microstructure Physics, Weinberg 2, Halle (Saale), Germany

ABSTRACT

Silicon ring resonator modulators (RRMs) have great potential to reduce footprint and power consumption and to increase modulation speeds in wavelength division multiplexed (WDM) transmitters. However, the optical properties of RRMs are highly sensitive to fabrication variations, which makes them challenging to design for volume production or a large number of WDM-channels. In this work, we present an RRM design that was specifically designed and experimentally validated to have reduced sensitivity to fabrication variations. This includes a sensitivity analysis of resist over- and under-exposure ($\pm$30 nm lateral dimension deviation) and of etch depth variability ($\pm$10 nm depth variation) within the coupling section. For our design, the deviation from the targeted coupling strength is improved twofold. The proposed devices are fabricated on SOI wafers using a standard CMOS-compatible process. We demonstrate RRMs with an extinction ratio above 5 dB, an OMA better that -7 dB (at 2 V_{pp}) and a 29 GHz electro-optical bandwidth, showing open eye diagrams at 32 Gb/s limited only by our measurement setup. The measured coupling coefficients are in good agreement with the simulated values. Furthermore, we applied the same design modifications to realize low-doped RRMs as well as ring based add-drop-multiplexers (OADMs). The agreement between the simulated and the measured coupling coefficients (that we identified as the main source of device performance variability) further confirms the effectiveness of our design modifications. These results suggest that the proposed design can be exploited to enable reliable fabrication of resonant-based devices on a large scale, especially in WDM systems.

Keywords: Silicon photonics, Ring modulators, Fabrication tolerance, WDM, Optical links.

1. INTRODUCTION

Resonance based devices in silicon-on-insulator (SOI) platforms, in particular resonant ring modulators (RRMs) at the transmitter and ring based optical add-drop multiplexers (OADMs) used as channel selection filters at the receiver, are widely exploited in wavelength division multiplexed (WDM) transceiver systems [1-4] due to their inherent wavelength selectivity, small footprint, and high energy efficiency [5,6]. However, their electro-optical (EO) properties, namely, EO bandwidth (BW) and modulation efficiency in the case of RRMs, highly depend on the coupling strength between the ring and the bus waveguide [7] and consequently on the design of the directional couplers. This imposes strict bounds to the process variations that can be tolerated while keeping the device performance in the targeted range. Thus, in order for these devices to be fabricated reliably in high volume using standard CMOS compatible processes, this process sensitivity must be kept at a minimum.

In this work, we present the design and implementation of high-speed silicon photonics (SiP) RRMs and OADMs with fabrication tolerant directional couplers. The paper is structured as follows. In Section 2, we present the design and simulation results of the fabrication-tolerant couplers, and compare field coupling coefficients (κ) extracted from two multi-project wafer (MPW) runs, both for RRMs and OADMs, to targeted values. In Section 3, we show the high-speed characterization of RRMs and OADMs that incorporate the fabrication tolerant directional coupler design.

*jnojic@iph.rwth-aachen.de; phone: +49 241 80 20030; www.iph.rwth-aachen.de

Silicon Photonics XV, edited by Graham T. Reed, Andrew P. Knights, Proc. of SPIE Vol. 11285, 112850A · © 2020 SPIE · CCC code: 0277-786X/20/$21 · doi: 10.1117/12.2543324

2. FABRICATION TOLERANT DIRECTIONAL COUPLERS: SIMULATION AND MEASUREMENTS

RRMs typically consist in doped Si rib waveguides to enable the electrical connectivity necessary for applying the modulating signal. The main sources of fabrication variabilities for this waveguide type are 1) over-/under-exposure of the photoresist, which results in the waveguide width deviating from its target and 2) the variability of the etch depth, leading to a change in slab thickness. Both of the affected geometrical features have a significant impact on the mode coupling between the bus waveguide and the ring, determining the coupling strength. This in turn simultaneously influences the EO modulation BW as well as the efficiency of the modulator, making it one of the parameters that are crucial to keep the device performance within specifications. We evaluate both of the aforementioned issues in our design, assuming ±30 nm waveguide width variation and ±10 nm slab height variation. To benchmark its tolerance to fabrication variations, we compare it with the conventional, commonly used directional coupler with a straight waveguide shown in Fig. 1(a) [8,9].

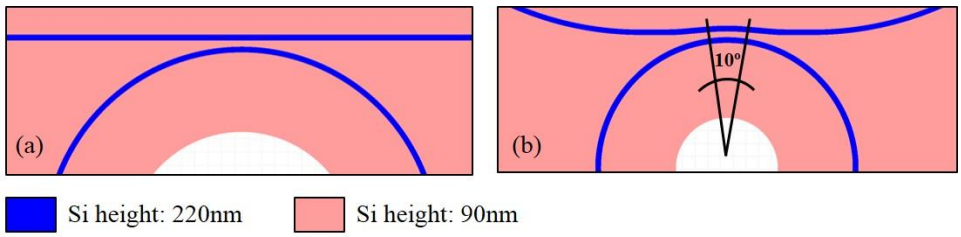

Fig. 1: Directional coupler geometry of (a) a conventional straight bus waveguide design; (b) our design with bent bus waveguide.

The top view of the coupling structure investigated here is depicted in Fig. 1(b). For both types of couplers, the ring radius is fixed to 10 µm to achieve the targeted free spectral range (FSR) of 9.8 nm ($n_g = 3.879$). As in the rest of the device, the directional coupler features rib waveguides with a targeted slab height of 90 nm.

In our design, the coupler section consists of a bent bus waveguide with a radius of curvature of 16 µm that is higher than that of the ring, covering an angular span of 10° in which the bus waveguide is progressively moved away from the ring. Outside of this coupling section, the curvature of the bus waveguide is progressively changed to route it away. An important benefit of such weakly tapered gap couplers that has been previously pointed out in the literature is that it provides a smoother transition between the sections where no coupling is present and the coupled region, which reduces the directional coupler excess loss [7,10]. It also enables a better phase matching between the modes in the coupling section.

Here, we investigate the improvement of coupling coefficient sensitivity against fabrication variations. The origin of that improvement in terms of etch depth variability is qualitatively illustrated in Fig. 2. The four panels (a)-(d) each show mode profiles for the bus waveguide and for the ring waveguide, as solved for an isolated waveguide core taking the bending radius into account, for four configurations consisting in either the straight waveguide or the weakly tapered gap configuration as well as in two slab thicknesses of 80 nm and 95 nm, that are respectively slightly below and slightly above the nominal 90 nm slab thickness. In general, the coupling strength between the ring and bus waveguides is proportional to the overlap between the two guided modes in the waveguide core regions (that respectively constitute a refractive index perturbation for the other waveguide). In a conventional coupler, in the case of e.g. under-etching, the ring mode becomes less confined and is pushed out towards the periphery of the ring and thus towards the bus waveguide. At the same time, the mode in the bus stays centered, while symmetrically expanding into the surrounding slab. The resulting changes in the modal profiles can be seen by comparing Figs. 2(a) and 2(b), wherein the vertical dashed lines serve as a guide to the eye. This can significantly increase the overlap and in turn the coupling strength between the two modes, resulting in a deviation from the targeted coupling strength κ. Conversely, the coupling strength reduces when the slab height is lower than intended. In contrast, in the proposed coupler, in the case of under-etching, the guided mode in the bus waveguide expands outwards as well, away from the ring waveguide, as seen in Fig. 2(d). This partially voids the excess overlap between the two modes, so that the sensitivity of the resulting coupling strength against etch depth variations is expected to be improved.

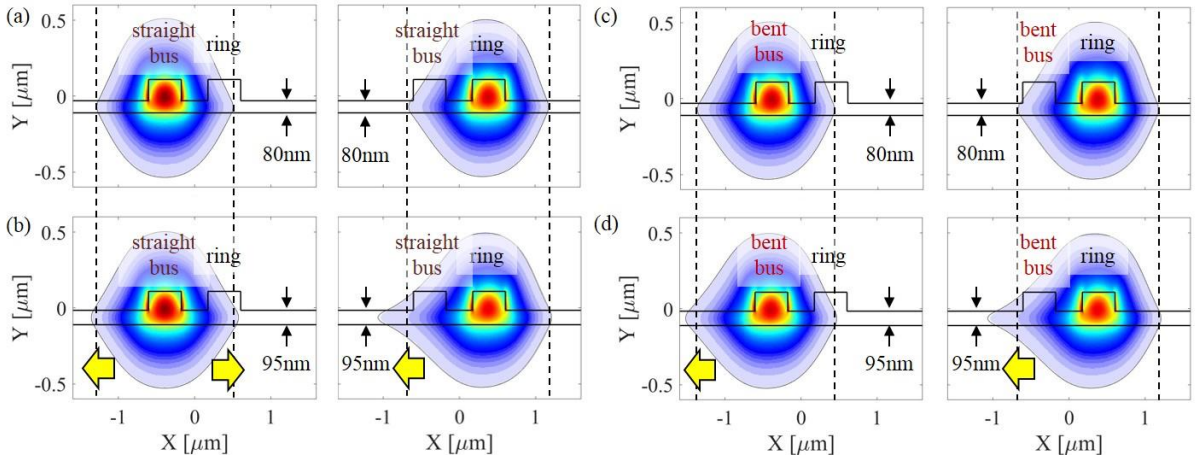

Fig. 2: Mode profiles at the RRM directional coupler inside of the bus waveguide (left graph in each panel) and the ring waveguide (right graph). The four panels correspond to couplers with a straight bus waveguide and (a) a 80 nm or (b) 95 nm slab height, as well as with a weakly tapered gap coupler and a (c) 80 nm or (d) 95 nm slab height. The yellow arrows show the directions in which the mode profiles expand when the slab thickness increases. The black contour line surrounding the modes corresponds to the location where the E-field has decayed to 1.5% of its maximum value. Vertical dashed lines serve as guides to the eye to compare the mode profiles before and after slab thickness modification.

To quantify the improvement achieved by the proposed coupler geometry, we simulated the coupler performance under various fabrication inaccuracies using the Lumerical FDTD toolbox for both types of couplers. The target coupling strength (κ=0.28) was chosen using the modeling process explained in detail in [11] so as to obtain an extinction ratio (ER) > 5 dB, an optical modulation amplitude of -7 dB, both for a drive voltage of 2 V_{pp}, and a BW of at least 20 GHz. This target coupling coefficient is indicated by dark crosses in Fig. 3. In the first step, we establish suitable values for the waveguide width and the gap between the bus waveguide and the ring to achieve the desired field coupling strength of 0.28. These are calculated to be 400 nm and 350 nm, respectively, in the case of a straight bus configuration, and 430 nm and 300 nm in the case of the bent bus waveguide.

In the second step, we calculate the coupling coefficient for various etch depths and over-/under-exposure of the photoresist. The latter is modeled by simultaneous variation of the waveguide width and of the gap, e.g. an under-exposure results in wider waveguides and a smaller gap size. The calculated values for the field coupling coefficient κ are shown in Fig. 3. Along each curve, the width and gap are jointly varied by ±30 nm. The same curves are then recalculated for the case of under-/over-etching. By comparing the corner values of our tolerance analysis – maximum over-exposure (i.e. the narrowest waveguide) at the lowest etch depth (i.e. the highest slab) with the maximum under-exposure (i.e. the widest waveguide) at the highest etch depth (i.e. the lowest slab) – we calculate a twofold reduction in the coupling coefficient variation when moving from the standard structure to the proposed design, from $\Delta\kappa \sim 0.098$ to $\Delta\kappa \sim 0.049$.

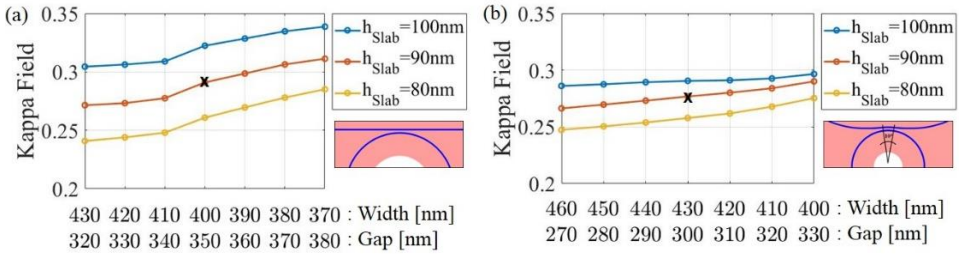

Fig. 3: Sensitivity analysis for the directional coupler with (a) straight bus waveguide and (b) bent bus waveguide.

The coupling strength, for a given gap size, is in general higher for narrower waveguides, since the guided modes are less confined. However, couplers with narrower waveguides are also more sensitive to variations in waveguide width, since

reduction of the waveguide width below 400 nm results in a rapid mode expansion which drastically increases the coupling coefficient. Therefore, we opted for a wider, less sensitive waveguide, moving to narrower gaps for achieving the same coupling strength, within our design constraints, i.e., the minimum gap feature size as well as satisfying the single mode condition at λ=1550 nm. Resulting gap requirements of 300 nm and 350 nm, respectively for the bent and the straight bus waveguide, are well within the capabilities of the 249 nm-deep ultra-violet (DUV) lithography used to fabricate the samples.

OADMs are another important element of on-chip WDM transceivers used for channel separation at the receiver. Acting as passive filters, they require no high-speed electrical connectivity, and therefore primarily consist in fully etched waveguides. This removes the variability due to the change in etch depth, leaving the over/under-exposure of the resist as the main fabrication variation to be considered. To tackle this, similarly as in the case of RRMs, we moved towards waveguides with wider widths, reducing the sensitivity to waveguide width variation. In order to achieve the desired coupling strength for the optimized width/gap combination without ending up with excessively small gaps, the length of the rectilinear section in a race-track configuration is increased accordingly.

Next, we measured numerous devices that include the fabrication tolerant directional couplers, both within the RRM and OADM structures, on several chips, in order to extract the resulting coupling coefficients. These chips were fabricated in two separate MPW runs at the Institute of Microelectronics (IME), A*STAR, Singapore. The micrograph of the fabricated RRMs and OADMs are shown in Figs. 4(a) and 4(c). The coupling strengths extracted from the measurements show good agreement with the simulated values, as can be seen in Fig. 4(b) for RRMs and Fig. 4(d) for OADMs. It should be noted that in our sensitivity analysis, we symmetrically reduced/increased the waveguide width, as well as the slab height in the RRM case, on both sides of the waveguide. The discrepancy for narrower gaps may, however, come from the process bias for smaller geometrical features, as we approach the critical dimension of the process, that will asymmetrically affect the gap region.

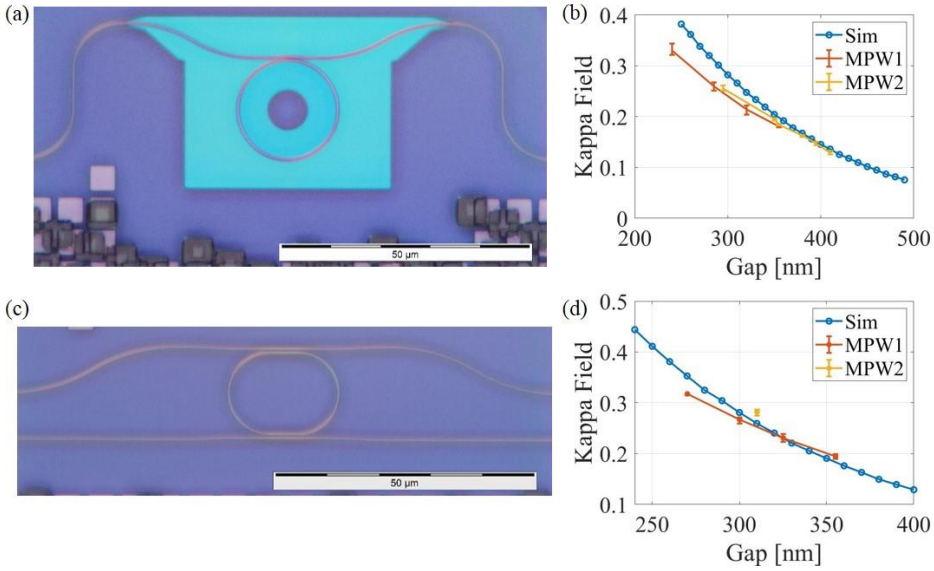

Fig. 4: (a) Micrograph of one type of RRM test structure; (b) comparison between the simulated (blue) and measured (red and yellow) values of the coupling coefficient for RRM directional couplers; (c) micrograph of one type of OADM test structure; (d) comparison between the simulated (blue) and measured (red and yellow) values of the coupling coefficient for OADM directional couplers.

3. HIGH SPEED DEVICE PERFORMANCE

Going one step further in our analysis, we tested the DC performance of the full RRM devices, as well as their EO BW and data transmission capacity, to show the applicability of the proposed coupler structure in high-speed devices. We

characterized the OADMs in terms of their EO BW and performed the data transmission experiments using an integrated SiP receiver in which they are used for channel dropping.

Fig. 5(a) shows the optical transfer functions of the RRMs for varying DC voltages applied in reverse bias to the high-speed carrier depletion phase shifters. The efficiency of the RRMs is described in terms of the optical modulation amplitude (OMA) and the extinction ratio (ER) for 2 V_{pp}, which are both wavelength dependent [12]. The values of OMA and ER versus wavelength are extracted from the transfer functions, and are shown in Fig. 5(b). We further measured the EO response of the device under small signal operation at 1 V reverse bias. The extracted, wavelength dependent -3 dB BW is shown in Fig. 5(c). The points that are indicated with a dark circle in Figs. 3(b) and 3(c) mark the bias point at which the device is tuned for transmission experiments. Multiple RRMs were measured on several chips, all showing performance within specifications, which includes OMA ≥ -7 dB, ER ≥ 5 dB, and EO BW ≥ 20 GHz for -1 V bias and a 2 V_{pp} voltage swing. According to their measured 3-dB EO BW, these devices can accommodate data rates > 50 Gb/s. In our data transmission experiments, we were, however, limited by the available equipment to the maximum data rate of 32 Gb/s [Fig. 5(d)].

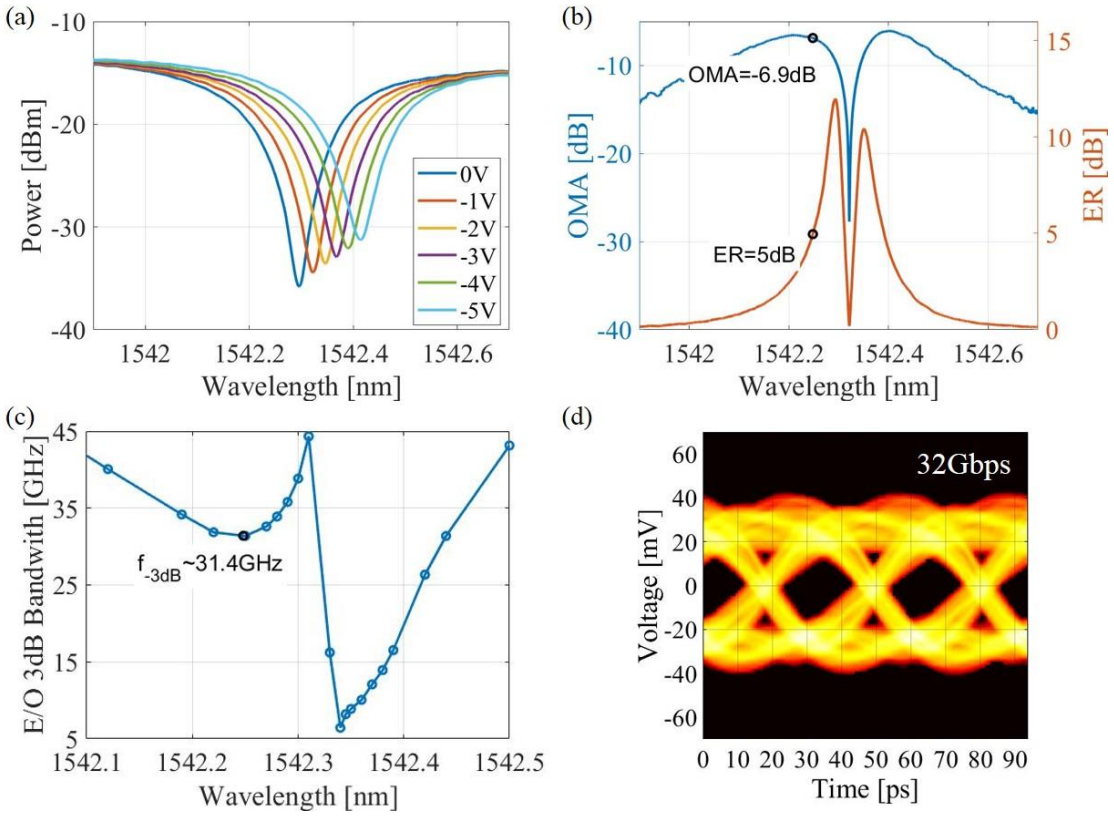

Fig. 5: (a) RRM wavelength sweeps for different applied DC voltages; (b) optical modulation efficiency (left axis) and extinction ratio (right axis) near the resonance frequency under the applied 2 V_{pp}; (c) wavelength dependent EO BW near the resonance frequency under 1V DC bias; (d) eye diagram at 32 Gb/s at the optimum detuning point.

The high-speed OADM measurements are shown in Fig. 6. Similarly to RRMs, the OADMs consistently exhibit the targeted EO BW ≥ 20 GHz with insertion loss (IL) < 2 dB across different chips. Alongside high-speed germanium waveguide photodiodes (BW~20 GHz), they are used in a receiver that allows for data transmission with data rates up to 25 Gb/s, as shown in Fig. 6(b).

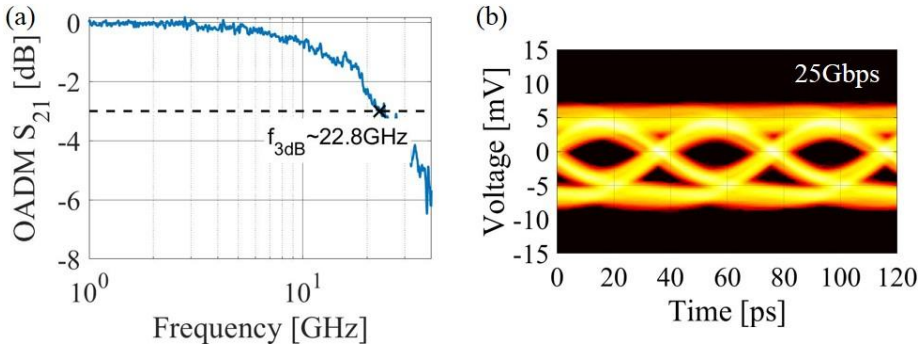

Fig. 6: (a) Measured OADM EO response; (b) eye diagram measured at 25 Gb/s using on-chip Ge photodetectors.

4. CONCLUSIONS

We have designed fabrication-tolerant RRMs with directional coupler sections that show a twofold reduction in sensitivity to fabrication variations that include ±30 nm variation in waveguide width and ±10 nm variation in slab height, when compared with the conventional straight bus waveguide coupler. Additionally, we modified the directional coupler of ring based OADMs to reduce their sensitivity to over-/under-exposure of the resist. Measured coupling strengths are in good agreement with simulated predictions for both types of devices. As a critical part of high-speed RRMs and OADMs, they allow for reliable and repeatable fabrication of WDM transceivers, as confirmed by the measurement of numerous devices across different chips and MPW runs. The RRMs consistently meet the targeted performance, with OMA > -7 dB, ER > 5 dB and EO BW > 20 GHz. The same stands for OADMs, that feature an expected EO BW > 20 GHz.

ACKNOWLEDGEMENTS

The authors would like to acknowledge support by the European Union for project BIG PIPES under contract number 619 591.

REFERENCES

[1] L. Luo, N. Ophir, C. Chen et al., "WDM-compatible mode-division multiplexing on a silicon chip," Nat. Commun. 5, 3069 (2014).
[2] A. Moscoso-Mártir et al., "8-channel WDM silicon photonics transceiver with SOA and semiconductor mode-locked laser," Opt. Express 26, 25446-25459 (2018).
[3] P. Dong, "Silicon Photonic Integrated Circuits for Wavelength-Division Multiplexing Applications," IEEE J. Sel. Top. Quantum Electron. 22(6), 370-378 (2016).
[4] A. Moscoso-Mártir et al., "Silicon Photonics Transmitter with SOA and Semiconductor Mode-Locked Laser," Sci. Rep. 7, 13857 (2017).
[5] M. Asghari and A. V. Krishnamoorthy, "Silicon photonics: Energy-efficient communication," Nat. Photon. 5(5), 268-270 (2011).
[6] J. Witzens, "High-Speed Silicon Photonics Modulators," Proceedings of the IEEE 106(12), 2158-2182 (2018).
[7] S. Romero-García et al., "High-speed resonantly enhanced silicon photonics modulator with a large operating temperature range," Opt. Express 42(1), 81-84 (2017).
[8] A. Ayazi, T. Baehr-Jones, Y. Liu, A. L. Lim, and M. Hochberg, "Linearity of silicon ring modulators for analog optical links," Opt. Express 20, 13115-13122 (2012).
[9] X. Zheng et al., "A high-speed, tunable silicon photonic ring modulator integrated with ultra-efficient active wavelength control," Opt. Express 22, 12628-12633 (2014).
[10] D. T. Spencer et al., "Integrated waveguide coupled Si_3N_4 resonators in the ultrahigh-Q regime," Optica 1(3), 153-157 (2014).
[11] J. Müller et al., "Silicon photonics WDM transmitter with single section semiconductor mode-locked laser," Adv. Opt. Technol. 4(2), 119-145 (2015).
[12] J. Müller et al., "Optical Peaking Enhancement in High-Speed Ring Modulators," Sci. Rep. 4, 6310 (2015).